Genetics in Medicine (2022) 24, 2249–2261

ELSEVIER

Genetics in Medicine
An Official Journal of the ACMG

www.journals.elsevier.com/genetics-in-medicine

ARTICLE

Biallelic *DAW1* variants cause a motile ciliopathy characterized by laterality defects and subtle ciliary beating abnormalities

ARTICLE INFO

Article history:
Received 23 November 2021
Received in revised form
20 July 2022
Accepted 20 July 2022
Available online 8 September 2022

Keywords:
DAW1
Heterotaxy
Left-right asymmetry
Motile cilia
Primary ciliary dyskinesia

ABSTRACT

Purpose: The clinical spectrum of motile ciliopathies includes laterality defects, hydrocephalus, and infertility as well as primary ciliary dyskinesia when impaired mucociliary clearance results in otosinopulmonary disease. Importantly, approximately 30% of patients with primary ciliary dyskinesia lack a genetic diagnosis.

Methods: Clinical, genomic, biochemical, and functional studies were performed alongside in vivo modeling of *DAW1* variants.

Results: In this study, we identified biallelic *DAW1* variants associated with laterality defects and respiratory symptoms compatible with motile cilia dysfunction. In early mouse embryos, we showed that *Daw1* expression is limited to distal, motile ciliated cells of the node, consistent with a role in left-right patterning. *daw1* mutant zebrafish exhibited reduced cilia motility and left-right patterning defects, including cardiac looping abnormalities. Importantly, these defects were rescued by wild-type, but not mutant *daw1*, gene expression. In addition, pathogenic *DAW1* missense variants displayed reduced protein stability, whereas DAW1 loss-of-function was associated with distal type 2 outer dynein arm assembly defects involving axonemal respiratory cilia proteins, explaining the reduced cilia-induced fluid flow in particle tracking velocimetry experiments.

Conclusion: Our data define biallelic *DAW1* variants as a cause of human motile ciliopathy and determine that the disease mechanism involves motile cilia dysfunction, explaining the ciliary beating defects observed in affected individuals.

Introduction

Cilia are hair-like microtubule-based projections from the plasma membrane extending into the extracellular space to perform wide-ranging developmental and physiological functions. Two main forms of cilia are defined according to their function; motile cilia that induce extracellular fluid movement and immotile (or sensory) cilia important for chemo-/mechano-sensory signaling.[1] Disorders arising because of ciliary malfunction (ciliopathies) comprise a genetically and clinically heterogeneous group of conditions typically involving variants in genes encoding core ciliary

Joseph S. Leslie, Rim Hjeij, and Asaf Vivante contributed equally and are joint first authors.

*Correspondence and requests for materials should be addressed to Emma L. Baple, Medical Research (Level 4), RILD Wellcome Wolfson Centre, Royal Devon & Exeter NHS Foundation Trust, Barrack Road, Exeter, EX2 5DW, United Kingdom. *E-mail address:* E.Baple@exeter.ac.uk OR Andrew H. Crosby, Medical Research (Level 4), RILD Wellcome Wolfson Centre, Royal Devon & Exeter NHS Foundation Trust, Barrack Road, Exeter, EX2 5DW, United Kingdom. *E-mail address:* A.H.Crosby@exeter.ac.uk OR Daniel T. Grimes, Institute of Molecular Biology, University of Oregon, Eugene, OR, 97403. *E-mail address:* DTGrimes@uoregon.edu

A full list of authors and affiliations appears at the end of the paper.

doi: https://doi.org/10.1016/j.gim.2022.07.019

molecular components.[2] Owing to the near ubiquitous expression of cilia and their functional diversity, ciliopathies may manifest a broad range of clinical features.

Disorders arising from defects in motile cilia are termed motile ciliopathies, which are characterized by varying combinations of clinical features depending on the specific genes involved and their tissue expression.[2] Motile cilia, positioned throughout the epithelium of the respiratory tract, sinuses, and middle ear, uniformly orientate to generate a monodirectional flow for mucociliary clearance.[3] Motile cilia dysfunction is frequently associated with primary ciliary dyskinesia (PCD), the most commonly recognized motile ciliopathy, characterized by severe recurrent otosinopulmonary disease caused by persistent mucus retention.[4] PCD is strongly associated with male infertility and laterality defects, including situs inversus (SI; mirror-image reversal) and situs ambiguous (heterotaxy).[4] Male infertility is caused by defects in sperm flagella, whereas laterality defects arise because of disruption of left-right (L-R) internal organ asymmetry, an evolutionarily conserved process in vertebrates initiated by motile cilia at the ventral node during embryonic development. These specialized cilia rotate to induce a leftward flow of embryonic fluid detected by immotile cilia around the node periphery,[5] inducing left-sided activation of the NODAL cascade.[6,7]

Many pathomolecular processes underlie nonsyndromic laterality defects, including impaired NODAL signaling (eg, DAND5[8,9]) and motile (eg, DNAH9[10]) and sensory cilia dysfunction (eg, PKD2[11]). However, along with otosinopulmonary PCD symptoms, laterality defects are invariably due to defective assembly, motility, or organization of motile cilia. Cilia motility is driven by inner dynein arms and outer dynein arms (ODAs), motor complexes that power sliding interactions between microtubules, with ODAs being the primary force generator. Ciliary import of preassembled ODAs is required for ciliary beating, a process shown to be mediated in green algae *Chlamydomonas reinhardtii* by intraflagellar transport component IFT46 and cargo adaptor ODA16.[12–14] The zebrafish ODA16 homolog (Wdr69) is required for motile cilia function in zebrafish,[15] as are its planarian (smed-DAW1)[16] and mammalian (DAW1)[17] homologs. Human and green algae DAW1/ODA16 crystal structures reveal highly similar β-propeller regions, with a conserved C-terminal ODA binding domain.[18,19] *Chlamydomonas* ODA16 associates with IFT46 via an N-terminal region, including the β-propeller, although, it remains unclear whether DAW1 exhibits a similar association.[18,19] In this study, we showed that biallelic *DAW1* variants cause a novel motile ciliopathy, characterized by laterality defects and subtle ciliary beating defects.

Material and Methods

Clinical and genetic studies

Affected individuals from family 1 were identified through their clinician as part of a larger study of laterality disorders in Anabaptist communities. To further characterize the genetic and clinical spectrum of *DAW1*-related disease, we explored GeneMatcher (https://genematcher.org), identifying a further Palestinian child (family 2). All genotyped individuals underwent echocardiography. Additional phenotypic information was obtained through the clinical care provider using a targeted clinical questionnaire, with written informed consent. DNA was extracted from blood/buccal samples using standard techniques. After the dideoxy sequencing exclusion of established Amish/Mennonite PCD and laterality defect founder variants (family 1, see Supplemental Methods),[20] exome sequencing (ES, family 1: 1-VII-1, 1-VII-5, 1-VII-8, family 2: 2-IV-1) was performed on Illumina platforms. Full sequencing methodology for each family is described in Supplemental Methods.

Variants with <5 reads and a frequency >0.5% in gnomAD (Genome Aggregation Database, v2.1.1) and/or in-house databases were excluded. Exonic or intron/exon boundary (±6 nucleotides of the splice junction), de novo (family 2), homozygous, or compound heterozygous variants were evaluated and prioritized by call quality, allele frequency, predicted functional consequence, and segregation with disease. All variants were then assessed for correlation with the clinical phenotype.

Unique primers were used for amplification and bidirectional dideoxy sequencing of all *DAW1* variants identified, which were deposited in ClinVar (SCV002025271 – SCV002025275).

Immunofluorescence analysis

Nasal brushings were obtained from all affected individuals. Immunofluorescence analysis was performed as previously described[21] (see Supplemental Methods for details).

In situ expression analysis

C57BL/6J mouse embryos were dissected after confirmation of mating by vaginal plugs. Fixed embryos (4% paraformaldehyde) were dehydrated using methanol. Whole mount in situ hybridization with an antisense digoxygenin-labeled *Daw1* riboprobe (594-1326 of sequence ENSMUST00000065436.9, Ensembl release 101) was performed following the standard protocols. Alkaline phosphatase–coupled antidigoxygenin antibody (Roche) was used to localize hybridized probes using NBT/BCIP (Roche). Zebrafish *dand5/myl7* in situ hybridization[22] used digoxygenin-labeled antisense probes generated from synthesized DNA templates through in vitro transcription (Roche) following the standard procedures for embryo imaging (THUNDER stereoscope, Leica).

Zebrafish

Embryos from natural matings (AB strain zebrafish) were incubated (28 °C). *daw1*^{b1403} CRISPR-Cas9 generated

mutants harboring an isoleucine-140/alanine-141 deletion exhibited loss-of-function phenotypes as previously described.[23] Daw1 messenger RNA (mRNA) synthesized from Daw1-encoding linearized plasmid (mMessage mMachine SP6 Transcription Kit, ThermoFisher Scientific) was purified using lithium chloride for injection (20 pg of wild-type [WT] Daw1 [Daw1^{WT}] or variant mRNA; site-directed mutagenesis, ThermoFisher Scientific) at the 1-cell stage. Heart looping was assessed at 36 to 48 hours after fertilization. For Kupffer's vesicle (KV) cilia imaging, embryos (somite stage 8-10) were dechorionated and mounted in No. 1.5 coverslip-bottomed Mattek chambers in low-melt 0.5% agarose with the dorsal-posterior side down. Live imaging (Nikon Eclipse Ti2 inverted microscope) captured 512 × 512 differential interference contrast images at 250 frames per second (ImageJ). Motility was visualized using temporal image correlation spectroscopy, a Fourier transform based strategy for time course data in which areas of an image with periodic fluctuations are brighter in intensity and correspond to motile cilia. The density of cilia motility, called the motile area, was then calculated as the area of a region of interest, which showed periodic fluctuations, corresponding to the area harboring motile cilia.

High speed video microscopy and particle tracking velocimetry

We obtained cell cultures from 2 affected individuals (1-VII-1, 1-VII-5) homozygous for the *DAW1* NM_178821.2:c.427A>G; p.(Asn143Asp) variant. In 1-VII-1 cells, we performed high speed video microscopy to analyze ciliary beating. In 1-VII-5 cells, we undertook particle tracking experiments to analyze the ability of affected cilia to generate monodirectional flow. Particle tracking velocimetry experiments/high speed video microscopy were performed as previously described[24] (see Supplemental Methods for details).

Results

Genetic and clinical studies

A total of 4 individuals from 2 families with rare predicted damaging biallelic *DAW1* variants were identified. The first family were part of a larger study investigating the spectrum and causes of laterality disorders in the Anabaptist community and the second were found through GeneMatcher. See Figure 1, Supplemental Table 1 and Supplemental Table 2 for family pedigrees and ES variant lists.

Family 1

We initially investigated 3 Mennonite female siblings (63-76 years) with features suggestive of mild PCD. Individual 1-VII-8 displayed SI without otosinopulmonary symptoms. Individual 1-VII-1 displayed SI and had a history of recurrent otitis media in childhood. Individual 1-VII-5 had normal situs but was reported to have had multiple episodes of lower respiratory tract infections throughout her life and a chronic wet cough since childhood, which is now productive, consistent with dysfunction of respiratory cilia. She also reported recurrent episodes of otitis media in early life. All 3 affected women had children, with no apparent reduced fertility or history of ectopic pregnancy. Systemic examination was otherwise unremarkable, and there was no evidence of craniofacial dysmorphism (see Table 1 for a summary of the core phenotypic features).

Dideoxy sequencing excluded all previously established Amish/Mennonite causes of PCD and/or laterality defects. To define the genetic cause of disease, ES was undertaken using DNA from all 3 affected individuals. Filtering of ES data using standard metrics identified a homozygous missense variant (*DAW1*, NM_178821.2:c.427A>G; p.(Asn143Asp), NC_000002.12:g.227893904A>G) as the only likely candidate cause of the disease. The *DAW1* c.427A>G; p.(Asn143Asp) variant is absent from population databases (gnomAD v2.1.1, v3.1.2 accessed on May 20, 2022), results in the substitution of a highly conserved residue (Figure 1), and is predicted to be damaging by multiple in silico tools. Modeling the variant in the crystal structure of human DAW1 determined that Asn143 is positioned on the β-propeller N-terminal face and that the Asn143Asp substitution leads to loss of hydrogen bonds between β-propeller blades 2 and 3, potentially disrupting local structure and affecting association with binding partners (Supplemental Figure 1). The variant cosegregates as appropriate in all family members, and as expected for a founder variant, it is also present in the Anabaptist (Amish/Mennonite) variant server (a population specific database comprising >10,000 exomes) at low allele frequency (0.002) and only in heterozygous state.

Family 2

An 8-year old Palestinian child with heterotaxy (2-IV-1) presented in infancy with hypoplastic left heart, mitral atresia, transposition of the great arteries, double outlet right ventricle, total anomalous pulmonary venous return, pulmonic stenosis, and bronchial SI. Abdominal ultrasound showed a transverse liver and right-sided spleen (Table 1, Figure 1, Supplemental Figure 2). Clinical examination was otherwise unremarkable, and chromosomal microarray analysis was normal. Trio ES analysis excluded variants in all known laterality disorder/PCD genes and identified a candidate homozygous nonsense *DAW1* variant (NM_178821.2: c.357G>A; p.(Trp119*), NC_000002.12:g.227893834 G>A) as the likely cause of the disease (Figure 1). The variant is absent from population databases (gnomAD v2.1.1, v3.1.2 accessed on May 20, 2021) and is only present in a single heterozygote in a database of >8000 regional exomes. Furthermore, no loss-of-function *DAW1* variants have ever been observed in the general population in a homozygous state.

The genetic findings in both families described in this article align with those of a previous study investigating potential genetic causes of unexplained congenital heart disease

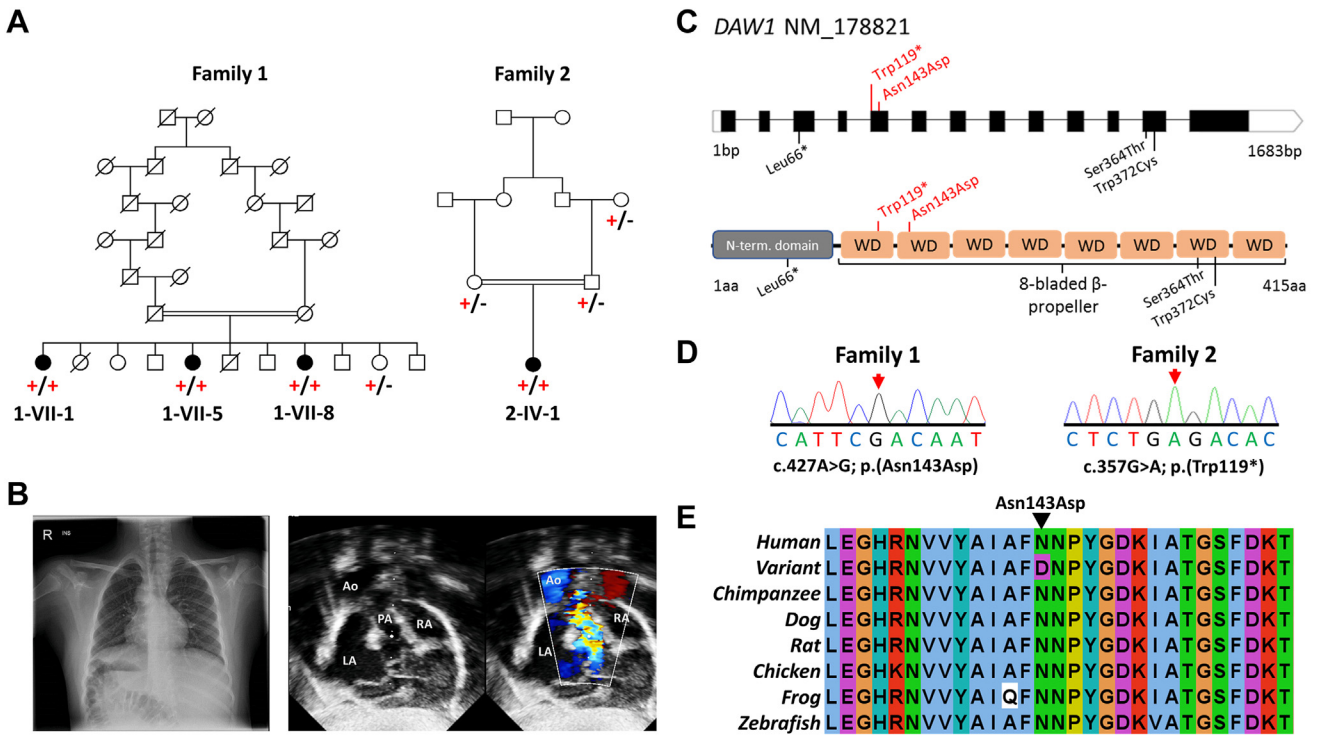

Figure 1 ***DAW1*** **variants, family pedigrees, and clinical images.** A. Simplified pedigree of the extended Mennonite family (family 1) and the Palestinian family (family 2) in which segregation of the [NM_178821.2:c.427A>G; p.(Asn143Asp)] and [NM_178821.2: c.357G>A; p.(Trp119*)] *DAW1* variants are indicated (+, variant; –, wild type). B. Chest radiograph from individual 2-IV-1 from family 2 showing the right sided aortic arch, right sided stomach, and situs inversus. Echocardiogram imaging from the same individual showing atrial situs inversus. C. Schematic showing *DAW1* intron–exon genomic organization (upper panel) and polypeptide domain architecture (lower panel), with position of DAW1 variants indicated. Variants identified in this study are indicated above the schematic in red, variants identified in previous studies are indicated below the schematic in black. D. Sequencing electropherograms from individuals homozygous for the p.(Asn143Asp) and p.(Trp119*) variants. E. Multiple sequence alignment of the Mennonite *DAW1* NM_178821.2:c.427A>G p.(Asn143Asp) variant; the substituted residue is indicated by the black arrow. Ao, aorta; LA, left atrium; PA, pulmonic artery; RA, right atrium.

in 2871 individuals.[25] In this study, biallelic *DAW1* variants identified in 2 individuals were proposed as the candidate cause of the disease. A homozygous *DAW1* missense variant (NM_178821.2:c.1091G>C; p.(Ser364 Thr), NC_000002.12:g.227921439G>C) was identified in a single individual with heterotaxy. This variant affects a highly conserved residue (Figure 1), is predicted damaging by multiple in silico tools, and is present at a low frequency in gnomAD v2.1.1 (0.00001591 accessed on May 20, 2022) and v3.1.2 (0.000006661 accessed on May 20, 2022), but not in homozygous state. Modeling the variant in the DAW1 crystal structure revealed that the side-chain hydroxyl group of Ser364 interacts with the side and main chain of Asp366 within blade 7 on the C-terminal face of the β-propeller, which is thought to bind ODAs (Supplemental Figure 1). A second individual with left ventricular obstruction was found to have inherited compound heterozygous *DAW1* (NM_17882 1.2:c.197T >A; p.(Leu66*), NC_000002.12:g.22788993 9T>A and NM_178821.2:c.1116G>T; p.(Trp372 Cys), NC_000002.12:g.227921464G>T) variants. Importantly, left ventricular obstruction may commonly occur in patients with heterotaxy, consistent with this individual being affected by a laterality defect. The Leu66* variant is present at a low frequency in gnomAD v2.1.1 (0.000008168, accessed on May 20, 2022) and v3.1.2 (0.000006571, accessed on May 20, 2022), but not in homozygous state, and is likely to result in nonsense mediated decay. The Trp372Cys substitution affects a highly conserved residue (Supplemental Figure 3), is predicted to be damaging by multiple in silico tools, and is absent from gnomAD (v2.1.1, v3.1.2, accessed on May 20, 2022). Notably, heterotaxy is frequently associated with defects in nodal cilia function and is observed in approximately 6% to 12% of patients with PCD.[26,27]

Ciliary beating is frequently impaired in motile ciliopathies. Therefore, we performed high speed video microscopy to analyze ciliary beating of a 15-day spheroid culture of cells from individual 1-VII-1 (family 1) (see Supplemental Methods). Compared with a control spheroid culture (Supplemental Video 1), multiciliated respiratory cells of 1-VII-1 showed a subtle reduction of the beating amplitude due to an impaired recovery stroke, which resulted in a stiff beating pattern (Supplemental Video 2). Moreover, to mimic the process of particle lung clearance in vitro, fluorescent particles were added to the apical compartment of the air liquid interface–transwell inserts to perform particle-tracking experiments with the cultivated

Table 1 Clinical findings of affected individuals homozygous or compound heterozygous for *DAW1* variants

Identifier	Ethnicity	Sex	Age, y	Laterality Defect	Congenital Heart Disease	Otosinopulmonary Features	Infertility	*DAW1* Genotype	Reference
1-VII-1	Mennonite	F	76	Situs inversus	–	Recurrent otitis media in childhood	–	p.(Asn143Asp)/ p.(Asn143Asp)	This study
1-VII-5	Mennonite	F	74	–	–	Chronic wet cough, recurrent lower respiratory infections, recurrent otitis media in childhood	–	p.(Asn143Asp)/ p.(Asn143Asp)	This study
1-VII-8	Mennonite	F	63	Situs inversus	–	–	–	p.(Asn143Asp)/ p.(Asn143Asp)	This study
2-IV-1	Palestinian	F	8	Situs ambiguous, transverse liver, right-sided spleen	Hypoplastic left heart, mitral atresia, transposition of the great arteries, double outlet right ventricle, total anomalous pulmonary venous return, pulmonary stenosis	–	NK	p.(Trp119*)/ p.(Trp119*)	This study
1-06817	NK	NK	NK	NK	Hypoplastic aortic annulus, hypoplastic left ventricle, left atrial hypoplasia, left sided patent ductus arteriosus, patent foramen ovale, sinus venosus septal defect, ventricular septal defect	NK	NK	p.(Leu66*)/ p.(Trp372Cys)	Jin et al[25]
1-01687	NK	NK	NK	Situs ambiguous, abdominal situs inversus	Atrial septal defect, biventricular discordant atrioventricular connection, discordant venticuloarterial connection, double outlet right ventriculoarterial connection, double outlet right ventricle, pulmonary stenosis, ventricular septal defect	NK	NK	p.(Ser364Thr)/ p.(Ser364Thr)	Jin et al[25]

Minus sign (–) indicates absence of a feature in an affected subject.
F, female; *NK*, not known.

respiratory epithelial cells from 1-VII-5 and a healthy control subject. Before every particle tracking experiment, a ciliary beat frequency (CBF) measurement of each insert under physiological conditions (37 °C) was performed to provide an overall impression of the inserts and to analyze the CBF. The CBF of 1-VII-5 with a mean of 9.21 ± 0.09 Hz was slightly increased compared with the healthy control (8.52 ± 0.09 Hz, $P = .035$). Particle tracking velocimetry experiments, including a group of 5 healthy controls resulted in a weighted mean particle velocity of 61.5 ± 3.7 μm/s. Cells from 1-VII-5 showed a particle velocity of 43.3 ± 2.2 μm/s, which is reduced by almost 30% compared with the healthy control group. The difference in velocity between the healthy control group and 1-VII-5 was 18.2 ± 4.3 μm/s. This translates into a significance of $P = .000027$. Overlay and polar graphs revealed that the particle flow was directed (Supplemental Figure 4) for both the healthy control group and 1-VII-5. In summary, we undertook 2 independent assessments investigating integrity of respiratory cilia function in which both showed subtle respiratory beating defects consistent with abnormal ciliary clearance of the airways.

DAW1 variants affect protein stability in vitro

To assess the effect of the *DAW1* variants on protein expression and stability, WT, p.Asn143Asp, and p.Ser364Thr missense alterations were expressed in insect cells and purified to assess unfolding temperature using nano differential scanning fluorimetry (see Supplemental Methods). Both alterations exhibited lower protein expression than WT in insect cells, indicative of impaired folding or stability. The third variant, p.Trp372Cys, was completely insoluble when overexpressed in insect cells, consistent with Trp372 being part of the DAW1 WD-repeat structure. WT DAW1 displayed an unfolding temperature of 75.4 °C (SD of 0.30 °C), whereas the p.Asn143Asp mutant DAW1 displayed a small reduction in unfolding temperature with 74.0 °C (4 SD below WT; Supplemental Figure 1B), indicating that protein stability is only modestly affected by the p.Asn143Asp substitution. Conversely, the p.Ser364Thr mutant DAW1 was found to be significantly destabilized, unfolding at a greatly reduced temperature of 59 °C (Supplemental Figure 1B).

Daw1 is expressed in the motile ciliated cells of the embryonic node in mice

PCD associated genes that cause laterality defects are required for motile cilia function in the embryonic node at approximately 3 weeks of gestation. To investigate *DAW1* expression, RNA in situ hybridization analysis was performed in mouse embryos at an equivalent developmental stage (early headfold to 6 somite stage). Mouse *Daw1* expression was evident in the node by the late headfold stage, reducing over the next few hours, consistent with a role in L-R determination (Supplemental Figure 5). Analysis of histologic sections revealed *Daw1* expression to be limited to the ventral node cells (Supplemental Figure 5). These cells exhibited motile cilia, consistent with DAW1 being directly involved in nodal cilia motility rather than other elements of the L-R determination pathway.

daw1 mutant zebrafish embryos exhibit reduced cilia motility and L-R patterning defects

To determine the effect of DAW1 loss-of-function in an animal model, L-R patterning in zebrafish $daw1^{b1403}$ mutants was investigated. $daw1^{b1403}$ mutants, generated using CRISPR/Cas9 mutagenesis,[23] harbor a 2-amino acid deletion in a conserved region (Figure 2A). Mutant embryos phenocopied previously published *daw1* morphants (embryos injected with morpholino oligonucleotides targeting *daw1*[15]). At 2 days post fertilization, $daw1^{b1403}$ mutants exhibited abnormal laterality of cardiac looping, indicative of defective L-R patterning (Figure 2B). Although control embryos showed dextral heart looping, $daw1^{b1403}$ mutant clutches contained embryos exhibiting either dextral or sinistral looping or, in some cases, failure of directional looping (Figure 2B). In zebrafish, organ asymmetry is determined by an L-R symmetry–breaking event that occurs in the KV, equivalent to the ventral node of mammals. Motile cilia within the KV generate an asymmetric fluid flow that is faster on the anterior-left side of the vesicle.[28,29] This results in repression of *dand5* on the left side of the KV, causing an R>L bias in *dand5* expression. This asymmetric expression was observed in control embryos (Figure 2C; $n = 28/30$). By contrast, $daw1^{b1403}$ mutants exhibited bilaterally equal *dand5* expression (Figure 2C; $n = 21/30$), showing that the L-R patterning defect in $daw1^{b1403}$ mutants lies upstream of asymmetric gene expression. To directly assess the cilia motility responsible for establishing L-R asymmetry, KV cilia were imaged using high-speed differential interference contrast microscopy at the 10-somite stage. In control embryos, KV cilia beat at 35.5 ± 2.4 Hz. In $daw1^{b1403}$ mutants, motility was almost entirely abolished (Figure 2D and Supplemental Video 3). Together, this showed that KV cilia motility is significantly disrupted in $daw1^{b1403}$ mutants, resulting in abnormal *dand5* asymmetric expression and cardiac laterality defects. These findings cohere with a previous zebrafish Daw1 knockdown study reporting motile cilia–associated developmental defects in Daw1 morphants.[15]

In vivo *DAW1* variant modeling

To assess the effect of *DAW1* variants on in vivo function, variant mRNAs were expressed in zebrafish embryos by 1-cell injection and after 36 to 48 hours incubation, cardiac looping laterality was determined. As earlier, uninjected $daw1^{b1403}$ mutants exhibited high levels of looping defects

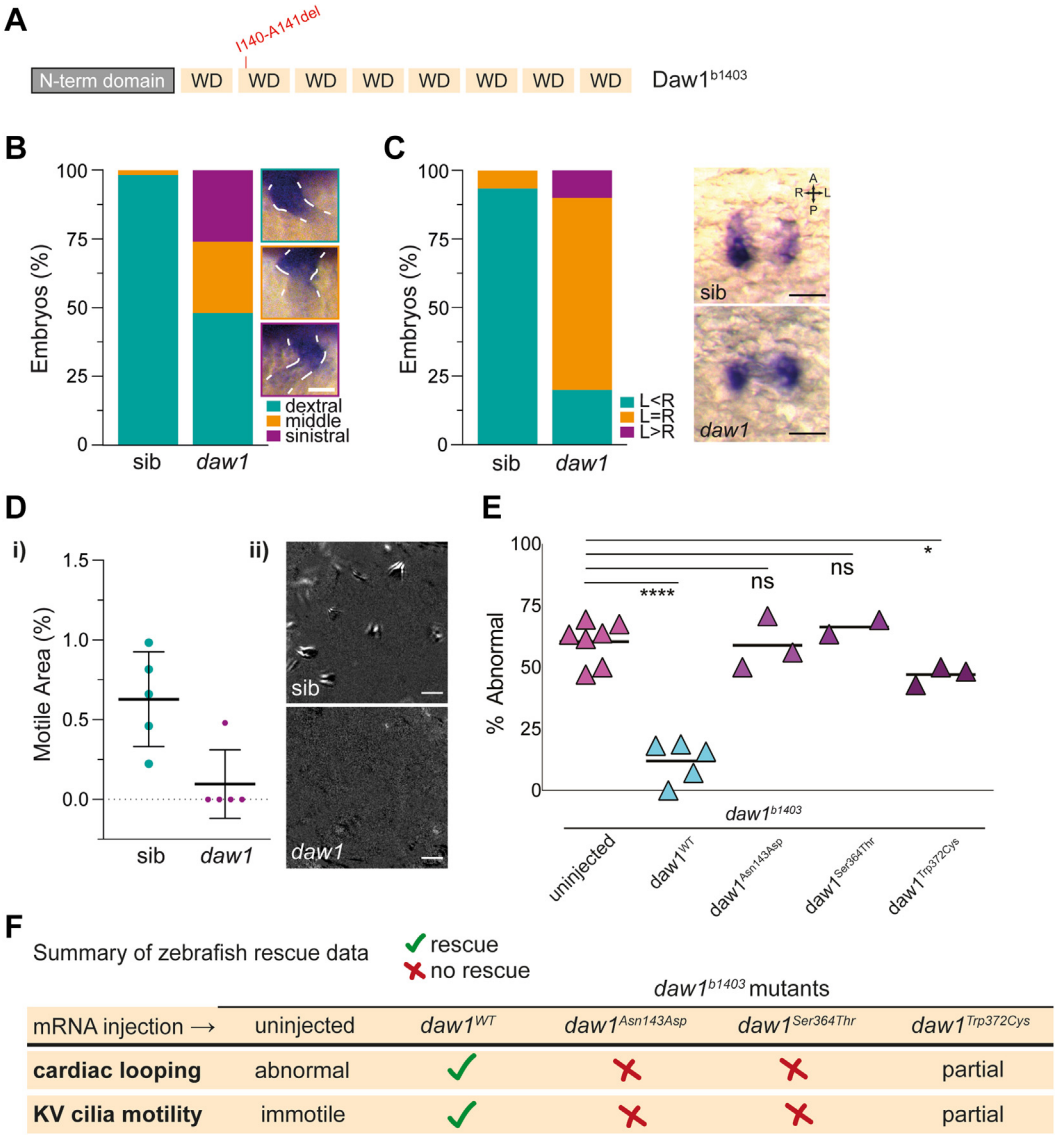

mRNA injection →	uninjected	*daw1*^{WT}	*daw1*^{Asn143Asp}	*daw1*^{Ser364Thr}	*daw1*^{Trp372Cys}
cardiac looping	abnormal	✓	✗	✗	partial
KV cilia motility	immotile	✓	✗	✗	partial

Figure 2 **In vivo modeling of *DAW1* variants using zebrafish mutant.** A. Schematic of zebrafish Daw1 protein showing the location of the 2 amino acid deletion present in *daw1*^{b1403} mutants. B. Quantitation of cardiac looping phenotypes with representative images in *daw1*^{b1403} mutants ($n = 54$) and sibling controls ($n = 118$). Scale bar: 50 μm. C. Quantitation of *dand5* expression with representative images in *daw1*^{b1403} mutants ($n = 30$) and sibling controls ($n = 30$). Scale bars: 50 μm. Di. Quantitation of the area occupied by motile cilia in KV at the 10-somite stage. Each data point represents a distinct embryo. Dii. Representative temporal image correlation spectroscopy images of KV cilia motility where white/gray pixels show regions of periodic motion. Scale bars: 5 μm. E. Dot plot showing the percentage of *daw1*^{b1403} mutant embryos exhibiting abnormal cardiac looping laterality after injections with mRNA encoding either wild-type or variant Daw1. *$P < .05$; ****$P < .001$; ns, not significant; unpaired *t* test was applied. F. Summary table of zebrafish rescue assay data. KV, Kupffer's vesicle; mRNA, messenger RNA; ns, not significant; sib, sibling control.

(58.9% ± 8.3% [mean ± SD], $N = 198$; Figure 2E). These defects were robustly rescued by mRNA injection encoding WT zebrafish Daw1, such that only 12.0% ± 8.2% of injected mutants exhibited looping laterality defects ($N = 78$). By contrast, zebrafish mRNA containing the p.Asn143Asp human variant failed to rescue mutants (59.0% ± 10.7%, $N = 101$; Figure 2E). Similarly, expression of p.Ser364Thr also failed to rescue mutants (66.4% ± 4.0%, $N = 21$; Figure 2E), whereas expression of p.Trp372Cys led to a partial but minor rescue (47.0% ± 3.7%, $N = 70$; Figure 2E). To directly assess the effect of human variant *daw1* expression on cilia motility, we imaged cilia in the KV. As earlier, *daw1*^{b1403} mutants lacked KV cilia motility, but this was rescued by injection of *daw1*^{WT} mRNA (Supplemental Videos 4 and 5). In agreement with our analysis of cardiac looping, expression of *daw1*^{Asn143Asp} and *daw1*^{Ser364Thr} failed to restore motility whereas *daw1*^{Trp372Cys} partially restored motility, resulting in cilia that beat slowly in the KV (Supplemental Videos 6-8). Our rescue data are summarized in Figure 2F. Overall, these data showed that all 3 missense mutations are loss-of-function, with p.Asn143Asp and p.Ser364Thr behaving as nulls in this context, whereas

p.Trp372Cys exhibited reduced but not completely abolished function.

DAW1 variants result in a variable partial defect in ODA assembly to ciliary axonemes

Defects in ODAs are the most frequently reported defects in PCD.[30] We have previously reported 2 types of ODAs in human: type 1 proximal, containing DNAH5 and DNAH11, and type 2 distal, containing DNAH5 and DNAH9.[31] Because DAW1 has been implicated in the transport of ODAs to the axonemes in lower organisms, we analyzed respiratory cilia from the 4 affected individuals with biallelic *DAW1* variants for defects in ODA assembly using immunofluorescence analysis. Analysis using antibodies targeting ODAs DNAH5,[32] DNAH9,[10] and the axonemal ODA intermediate chains DNAI1[33] and DNAI2[34] confirmed normal axonemal localization of the 4 ODA proteins in the respiratory cilia of controls and in affected individual 1-VII-8 (*DAW1* p.[Asn143Asp] homozygote). Conversely, in respiratory cells from individual 2-IV-1 (*DAW1* p.[Trp119*] homozygote), DNAH5, DNAI1, and DNAI2 assembled only to the proximal part of the ciliary axonemes in 62% (n [proximal] = 23, n [total] = 37), 56% (n [proximal] = 19, n [total] = 34), and 61% (n [proximal] =16, n [total] = 26) of cells, respectively, and DNAH9 was absent from 71% (n [mislocalized] = 15, n [total] = 21) of the cells (Figure 3), indicating a variable defect in type 2 ODA assembly in respiratory cells of this individual. We also analyzed cells from all 4 individuals using antibodies targeting CCDC114, an ODA docking component that anchors ODAs to microtubules.[35] We observed normal localization in all individuals (Supplemental Figure 6). Normal axonemal localization of nexin dynein regulatory complex component GAS8 (Figure 3), the inner dynein arm light chain DNALI1, and the ODA heavy chain DNAH11 (Supplemental Figure 7) confirmed the absence of other ciliary ultrastructure defects due to *DAW1* variants. In addition, because affected individuals presented with mild respiratory symptoms and laterality defects, we analyzed CFAP53,[36] ENKUR, and MNS1[20,37] localization, whose deficiency causes a similar human phenotype. All 3 proteins localized normally in 1-VII-8 and 2-IV-1 (Supplemental Figure 8), indicating that DAW1 most likely resides within a different molecular complex.

Together these findings indicated that DAW1 variants may result in a variable defect in ODA assembly to the distal portion of the axonemes, explaining the mild respiratory symptoms in some affected individuals and the modestly reduced speed and displacement of particles in particle tracking analysis.

Discussion

The most common and widely recognized motile ciliopathy is PCD, characterized by severe recurrent otosinopulmonary disease caused by impaired mucociliary clearance in combination with other variable features, including laterality defects and male infertility.[1,4] A combination of diagnostic tests, including nasal nitric oxide measurement, ciliary biopsy with electron microscopy, and ciliary beat analysis using high-speed video microscopy, may be used to diagnose PCD. However, none are comprehensive, and mild presentations will frequently go undiagnosed. Patients who lack otosinopulmonary features of PCD but present with SI or heterotaxy further complicate diagnosis.[38]

Although >40 ciliary genes are associated with PCD and laterality defects, variants in these genes explain only approximately 70% of the PCD cases.[39] Recently, an increasing number of novel genetic disorders have been described in which motile cilia dysfunction is associated with varying combinations of clinical features seen in PCD.[40] Indeed, several disease genes, including *MNS1*, *CFAP53*, and *DNAH9* have been associated with motile ciliopathy disorders typified by laterality defects and male infertility but do not fulfill PCD diagnostic criteria.[10,20,36,37]

In this article, we present genetic, clinical, functional, and animal-model data delineating a novel motile ciliopathy caused by DAW1 deficiency and characterized by laterality defects and subtle ciliary beating defects. Owing to its known role in cilia motility and the phenotype in mouse and zebrafish models, *DAW1* variants have previously been proposed as a potential cause of PCD,[15] although no conclusive association with human disease has been made. The variable otosinopulmonary features in affected family members in our study included a chronic wet cough and otitis media. Laterality defects were present in 3 of 4 individuals, with 2 presenting with SI and 1 presenting with heterotaxy. Particle tracking analysis of respiratory cilia revealed slightly reduced particle speed and displacement in 1 individual with recurrent lower respiratory tract infections (1-VII-5) when compared with healthy controls, indicative of impaired mucociliary clearance. Similar mild otosinopulmonary phenotypes with prominent laterality defects have previously been reported in individuals with CFAP53[36] and DNAH9-related ciliopathy disorders.[10] Jin et al[25] previously described 2 individuals presenting with congenital heart disease compatible with a laterality defect, in whom biallelic *DAW1*, homozygous p.(Ser364Thr), compound heterozygous p.(Leu66*)/p.(Trp372Cys) variants were proposed as candidate causes of disease. It is not known whether either patient exhibited otosinopulmonary features or reduced fertility. All 4 patients recruited to this study were female, and thus male infertility, a frequent feature of motile ciliopathies, could not be assessed. However, *DAW1* is highly expressed in the testis (GTex, accessed on November 11, 2021), and clinical phenotypes of similar ciliary genes often include male infertility. It is therefore possible that the full spectrum of *DAW1*-related disease may include male infertility, this will be clarified as more affected individuals are identified.

Our data showed that *Daw1* is expressed at the node in mouse embryos, consistent with a role in determining L-R

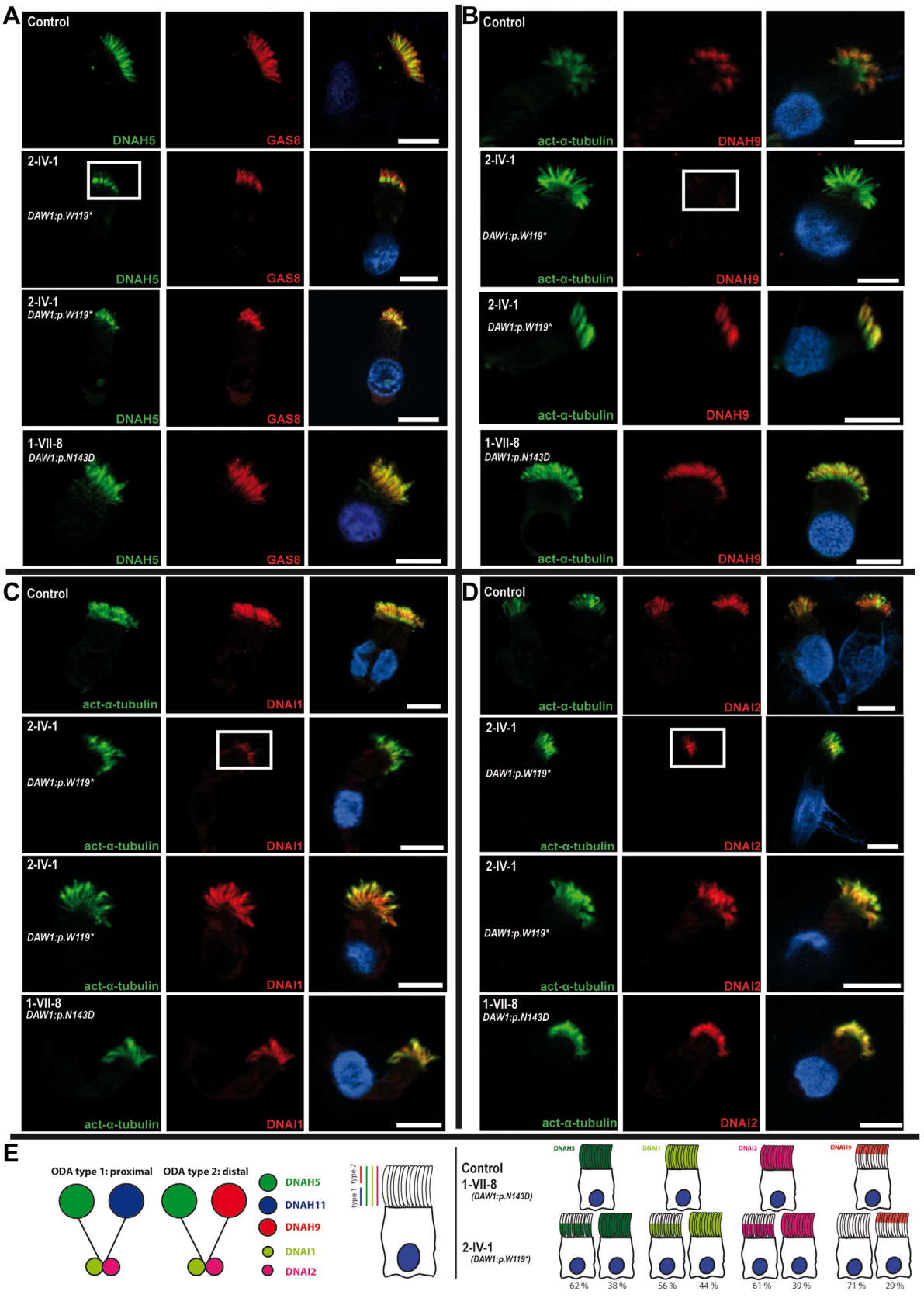

Figure 3 ***DAW1*** **loss-of-function variants cause a variable partial defect in the assembly of the outer dynein arm components DNAH5, DNAH9, DNAI1, and DNAI2 to the ciliary axonemes.** A-D. Respiratory epithelial cells derived from the affected Palestinian child (2-IV-1) homozygous for *DAW1* NM_178821.2: c.357G>A; p.(Trp119*), a Mennonite individual (1-VII-8) homozygous for *DAW1* variant NM_178821.2:c.427A>G; p.(Asn143Asp) and an unrelated control. Cells were double-labeled with antibodies directed against

asymmetry.[41] Furthermore, *Daw1* expression is limited to the motile ciliated cells in the node pit and does not extend to the sensory cilia at the node periphery. Congruous with this, *daw1*^{b1403} zebrafish mutants exhibited anatomical and molecular L-R defects owing to significantly reduced KV cilia motility, confirming an essential role for DAW1 in L-R asymmetry through motile cilia function and consistent with the human phenotype. Importantly, although WT Daw1 robustly rescued mutant *daw1*^{b1403} zebrafish laterality defects, neither the Asn143Asp/Ser364Thr, nor the Trp372Cys substitutions displayed rescue ability confirming that they result in loss-of-DAW1 function.

Previous studies in mice, zebrafish, and algae identified DAW1 as a likely contributor to the intraflagellar transport of ODAs.[13,15,18,42,43] In algae, DAW1 interacts with IFT46, which together bind and chaperone assembled ODAs into the ciliary axoneme.[18] Given the high sequence conservation and structural similarity of algae and human DAW1, it seems likely that it performs a similar functional role in mammalian motile cilia. In humans, 2 types of ODAs exist: type 1 proximal, composed of heavy chains DNAH5 and DNAH11, and type 2 distal, composed of heavy chains DNAH5 and DNAH9. In this study, we found that DAW1 deficiency led to a variable defect in the assembly of human type 2 ODAs to ciliary axonemes, with some cells displaying normal ODA assembly, indicating that DAW1 function in humans is likely partly compensated by other molecular components. As recently reported, DNAH9 variants leading to a complete loss of type 2 ODAs from ciliary axonemes result in milder forms of PCD.[10] The occasional absence of type 2 ODAs due to biallelic *DAW1* variants is thus consistent with the mildly impaired mucociliary clearance and respiratory symptoms observed.

Previously *Daw1*-deficient mice have been shown to exhibit a mild PCD phenotype, including laterality defects with striking similarities to those observed in the affected individuals described in this article. Solomon et al[17] observed that the ciliated area in *Daw1*$^{-/-}$ mice was not reduced compared with WT animals, with high-speed video microscopy showing robust ciliary motion. Despite this, *Daw1*$^{-/-}$ mice displayed impaired mucociliary clearance, postulated to be due to dyskinetic ciliary motion, with an abnormal stroke pattern. In addition, *Daw1*$^{-/-}$ mouse cilia displayed a reduced angle of effective stroke. The subtle ciliary beating defects and reduced mucociliary clearance observed in affected individuals in our study are consistent with these mice findings. Together, the data presented in this article conclusively define pathogenic biallelic *DAW1* variants as a cause of a new motile ciliopathy disorder characterized by laterality defects and mild respiratory symptoms due to subtle ciliary beating defects. Thus, *DAW1* gene analysis should be performed in individuals with heterotaxia and features suggestive of otosinopulmonary disease. Awareness of *DAW1*-related disease and the wider growing group of motile ciliopathies, in which heterotaxia is associated with mild but chronic respiratory symptoms, will improve treatment and reduce preventable lung disease.

Data Availability

The variants listed in this paper have been submitted to ClinVar (SCV002025271- SCV002025275).

Acknowledgments

First and foremost, we are grateful to the families for taking part in this study and to the Anabaptist communities and colleagues at the New Leaf Centre, Clinic for Special Children (Ohio), for their continued support to our work. The authors thank the Anabaptist Variant Server (AVS) collaborators: Regeneron Genetics Center, University of Maryland School of Medicine Amish Program, Clinic for Special Children, Das Deutsche Clinic, National Institute of Mental Health Amish Program and University of Exeter Windows of Hope Project for providing summary measures from genomic data. We thank Professor Orly Elpeleg and colleagues, Department of Genetics, Hadassah Medical Center, Israel, for providing allele frequency data for genetic variants. We also thank Judy Peirce for zebrafish husbandry as well as the Aquatics Facility and the GC3F Imaging Facility at the University of Oregon. We are grateful to Andreas Borgscheiper for the technical assistance in human cell culture and video microscopy. This work was supported by the Medical Research Council G1001931 (E.L.B.), MC_U142670370 (D.P.N.), MRC Proximity to Discover and Confidence in Concept grants (MC-PC-18047, MC_PC_15054, MC_PC_15047) to University of Exeter, E.L.B, and A.H.C.; Newlife Foundation for Disabled Children to E.L.B. and A.H.C.; the National Institutes of Health

DNAH5 (green, A), GAS8 (red, A), DNAH9 (red, B), DNAI1 (red, C), DNAI2 (red, D), and acetylated alpha-tubulin (green, B, C, and D). Nuclei were stained using Hoechst 33342 (blue). In an unaffected control and affected individual 1-VII-8, DNAH5, DNAI1, and DNAI2 localized to the whole axonemal length and DNAH9 localized to the distal compartment of the axonemes. However, in affected individual 2-IV-1, DNAH5, DNAI1, and DNAI2 only localized to the proximal part of the ciliary axonemes in a proportion of the analyzed cells; 62%, 56%, and 61%, respectively, and DNAH9 was absent in 71% of the cells (white box), indicating that recessive loss-of-function variants in *DAW1* variably affect the distal localization of ODA proteins. Scale bars: 10 μm. E. (Left side) Schematic showing the 2 types of ODAs in human: ODA type 1 localized to the proximal part of the cilia and contains DNAH5 and DNAH11 and ODA type 2 localized to the distal part of the cilia and contains DNAH5 and DNAH9. Both types contain the intermediate chains DNAI1 and DNAI2. (Right side) Schematic highlights the distal loss of DNAH5, DNAI1, DNAI2, and DNAH9 from the ciliary axonemes of affected individual 2-IV:1 with the corresponding percentages. ODA, outer dynein arm.

grants R00AR70905 (D.T.G.), R35GM142949 (D.T.G.), F32AR070082 (E.A.B.), and T32HD007348 (Z.H.I.); the Deutsche Forschungsgemeinschaft DFG HJ7/1-1 (R.H.); a Knight Campus Undergraduate Scholarship (S.B.C.); and a Donald E. and Delia B. Baxter Foundation Award (D.T.G.). A.V. is supported by an Israel Science Foundation (ISF) – Clinical Scientist Grant (grant number: 2773/19). E.L. would like to acknowledge Riisfort-Fonden and Toyota-Fonden, Denmark, for generous support to ciliopathy related projects. The Yale Center for Mendelian Genomics (NIH M#UM1HG006504) is funded by the National Human Genome Research Institute and the National Heart, Lung, and Blood Institute. The GSP Coordinating Center (U24 HG008956) contributed to cross-program scientific initiatives and provided logistical and general study coordination. The content is solely the responsibility of the authors and does not necessarily represent the office.

Author Information

Conceptualization: E.L.B., A.H.C., D.T.G., H.O., Y.A., D.P.N., E.L.; Formal Analysis: J.S.L., R.H., A.V., E.A.B., L.D., J.W.; Investigation: J.S.L., R.H., A.V., E.A.B., L.D., J.W., L.R., J.Ke., S.G., Z.H.I., S.B.C., J.Ko., B.P.-S., Y.B., O.B., S.M., K.K.F., O.W., E.S., H.E.C.; Writing-original draft: J.S.L., R.H., A.V., E.A.B., B.P.-S., E.L., D.P.N., Y.A., H.O., A.H.C., D.T.G., E.L.B.; Writing-review and editing: J.S.L., R.H., E.A.B., A.V., L.D., E.L., D.P.N., H.O., Y.A., D.T.G., A.H.C., E.L.B.

Ethics Declaration

Ethical approval for this project is from Akron Children's Hospital (#986876), University of Arizona (IRB – 1000000050), University of Exeter Medical School, and the Institutional Review Board of Sheba Medical Center (#7786-10). Written informed consent was obtained in all cases from patients or from a responsible parent in the case of children. Zebrafish experiments were undertaken in accordance with research guidelines of the International Association for Assessment and Accreditation of Laboratory Animal Care and approved by the University of Oregon Institutional Animal Care and Use Committee. Ethical approval for all mouse work was obtained from the UK Home Office and experiments were carried out in accordance with the Medical Research Council MRC Harwell Ethics Committee. All mouse colonies were maintained in a pathogen-free environment at the Mary Lyon Centre, MRC Harwell Institute.

Conflict of Interest

The authors declare no conflicts of interest.

Additional Information

The online version of this article (https://doi.org/10.1016/j.gim.2022.07.019) contains supplementary material, which is available to authorized users.

Authors

Joseph S. Leslie[1], Rim Hjeij[2], Asaf Vivante[3,4], Elizabeth A. Bearce[5], Laura Dyer[6], Jiaolong Wang[7], Lettie Rawlins[1,8], Joanna Kennedy[1], Nishanka Ubeyratna[1], James Fasham[1,8], Zoe H. Irons[5], Samuel B. Craig[5], Julia Koenig[2], Sebastian George[2], Ben Pode-Shakked[3,9], Yoav Bolkier[3,10], Ortal Barel[3,11,12], Shrikant Mane[13], Kathrine K. Frederiksen[7], Olivia Wenger[14], Ethan Scott[14], Harold E. Cross[15], Esben Lorentzen[7], Dominic P. Norris[6], Yair Anikster[3,9,12], Heymut Omran[2], Daniel T. Grimes[5,*], Andrew H. Crosby[1,*], Emma L. Baple[1,8,*]

Affiliations

[1]Institute of Biomedical and Clinical Science, RILD Wellcome Wolfson Centre, University of Exeter Medical School, Royal Devon University Healthcare NHS Foundation Trust, Exeter, United Kingdom; [2]Department of General Pediatrics, University Hospital Muenster, Muenster, Germany; [3]Sackler Faculty of Medicine, Tel Aviv University, Tel Aviv, Israel; [4]Department of Pediatrics B and Pediatric Nephrology Unit, Edmond and Lily Safra Children's Hospital, Sheba Medical Center, Ramat Gan, Israel; [5]Institute of Molecular Biology, University of Oregon, Eugene, OR; [6]MRC Harwell Institute, Harwell Campus, Oxfordshire, Oxford, United Kingdom; [7]Department of Molecular Biology and Genetics, Aarhus University, Aarhus, Denmark; [8]Peninsula Clinical Genetics Service, Royal Devon University Healthcare NHS Foundation Trust, Exeter, United Kingdom; [9]Metabolic Disease Unit, Edmond and Lily Safra Children's Hospital, Sheba Medical Center, Ramat Gan, Israel; [10]Pediatric Heart Institute, Edmond and Lily Safra Children's Hospital, Sheba Medical Center, Ramat Gan, Israel; [11]The Genomic Unit, Sheba Cancer Research Center, Sheba Medical Center, Ramat Gan, Israel; [12]Wohl Institute for Translational Medicine, Sheba Medical Center, Ramat Gan, Israel; [13]Department of Genetics, Yale School of Medicine, New Haven, CT; [14]New Leaf Center Clinic for Special Children, Mt Eaton, OH; [15]Department of Ophthalmology and Vision Science, University of Arizona College of Medicine, University of Arizona, Tucson, AZ

References

1. Horani A, Ferkol TW. Primary ciliary dyskinesia and associated sensory ciliopathies. *Expert Rev Respir Med.* 2016;10(5):569-576. http://doi.org/10.1586/17476348.2016.1165612

2. Waters AM, Beales PL. Ciliopathies: an expanding disease spectrum. *Pediatr Nephrol*. 2011;26(7):1039-1056. http://doi.org/10.1007/s00467-010-1731-7
3. Bustamante-Marin XM, Ostrowski LE. Cilia and mucociliary clearance. *Cold Spring Harb Perspect Biol*. 2017;9(4):a028241. http://doi.org/10.1101/cshperspect.a028241
4. Leigh MW, Pittman JE, Carson JL, et al. Clinical and genetic aspects of primary ciliary dyskinesia/Kartagener syndrome. *Genet Med*. 2009;11(7):473-487. http://doi.org/10.1097/GIM.0b013e3181a53562
5. Dasgupta A, Amack JD. Cilia in vertebrate left-right patterning. *Philos Trans R Soc Lond B Biol Sci*. 2016;371(1710):20150410. http://doi.org/10.1098/rstb.2015.0410
6. Shiratori H, Hamada H. TGFbeta signaling in establishing left-right asymmetry. *Semin Cell Dev Biol*. 2014;32:80-84. http://doi.org/10.1016/j.semcdb.2014.03.029
7. Grimes DT, Burdine RD. Left-right patterning: breaking symmetry to asymmetric morphogenesis. *Trends Genet*. 2017;33(9):616-628. http://doi.org/10.1016/j.tig.2017.06.004
8. Maerker M, Getwan M, Dowdle ME, et al. Bicc1 and Dicer regulate left-right patterning through post-transcriptional control of the Nodal inhibitor Dand5. *Nat Commun*. 2021;12(1):5482. http://doi.org/10.1038/s41467-021-25464-z
9. Cristo F, Inácio JM, de Almeida S, et al. Functional study of DAND5 variant in patients with Congenital Heart Disease and laterality defects. *BMC Med Genet*. 2017;18(1):77. http://doi.org/10.1186/s12881-017-0444-1
10. Loges NT, Antony D, Maver A, et al. Recessive DNAH9 loss-of-function mutations cause laterality defects and subtle respiratory ciliary-beating defects. *Am J Hum Genet*. 2018;103(6):995-1008. http://doi.org/10.1016/j.ajhg.2018.10.020
11. Bataille S, Demoulin N, Devuyst O, et al. Association of PKD2 (polycystin 2) mutations with left-right laterality defects. *Am J Kidney Dis*. 2011;58(3):456-460. http://doi.org/10.1053/j.ajkd.2011.05.015
12. Ahmed NT, Mitchell DR. ODA16p, a Chlamydomonas flagellar protein needed for dynein assembly. *Mol Biol Cell*. 2005;16(10):5004-5012. http://doi.org/10.1091/mbc.e05-07-0627
13. Ahmed NT, Gao C, Lucker BF, Cole DG, Mitchell DR. ODA16 aids axonemal outer row dynein assembly through an interaction with the intraflagellar transport machinery. *J Cell Biol*. 2008;183(2):313-322. http://doi.org/10.1083/jcb.200802025
14. Hou Y, Qin H, Follit JA, Pazour GJ, Rosenbaum JL, Witman GB. Functional analysis of an individual IFT protein: IFT46 is required for transport of outer dynein arms into flagella. *J Cell Biol*. 2007;176(5):653-665. http://doi.org/10.1083/jcb.200608041
15. Gao C, Wang G, Amack JD, Mitchell DR. Oda16/Wdr69 is essential for axonemal dynein assembly and ciliary motility during zebrafish embryogenesis. *Dev Dyn*. 2010;239(8):2190-2197. http://doi.org/10.1002/dvdy.22355
16. Lesko SL, Rouhana L. Dynein assembly factor with WD repeat domains 1 (DAW1) is required for the function of motile cilia in the planarian Schmidtea mediterranea. *Dev Growth Differ*. 2020;62(6):423-437. http://doi.org/10.1111/dgd.12669
17. Solomon GM, Francis R, Chu KK, et al. Assessment of ciliary phenotype in primary ciliary dyskinesia by micro-optical coherence tomography. *JCI Insight*. 2017;2(5):e91702. http://doi.org/10.1172/jci.insight.91702
18. Taschner M, Mourão A, Awasthi M, Basquin J, Lorentzen E. Structural basis of outer dynein arm intraflagellar transport by the transport adaptor protein ODA16 and the intraflagellar transport protein IFT46. *J Biol Chem*. 2017;292(18):7462-7473. http://doi.org/10.1074/jbc.M117.780155
19. Wang J, Taschner M, Petriman NA, et al. Purification and crystal structure of human ODA16: implications for ciliary import of outer dynein arms by the intraflagellar transport machinery. *Protein Sci*. 2020;29(6):1502-1510. http://doi.org/10.1002/pro.3864
20. Leslie JS, Rawlins LE, Chioza BA, et al. MNS1 variant associated with situs inversus and male infertility. *Eur J Hum Genet*. 2020;28(1):50-55. http://doi.org/10.1038/s41431-019-0489-z
21. Hjeij R, Onoufriadis A, Watson CM, et al. CCDC151 mutations cause primary ciliary dyskinesia by disruption of the outer dynein arm docking complex formation. *Am J Hum Genet*. 2014;95(3):257-274. http://doi.org/10.1016/j.ajhg.2014.08.005
22. Grimes DT, Patterson VL, Luna-Arvizu G, Schottenfeld-Roames J, Irons ZH, Burdine RD. Left-right asymmetric heart jogging increases the robustness of dextral heart looping in zebrafish. *Dev Biol*. 2020;459(2):79-86. http://doi.org/10.1016/j.ydbio.2019.11.012
23. Bearce EA, Irons ZH, Craig SB, et al. Daw1 regulates the timely onset of cilia motility during development. *Development*. 2022;149(12):dev200017. http://doi.org/10.1242/dev.200017
24. Wallmeier J, Frank D, Shoemark A, et al. De novo mutations in FOXJ1 result in a motile ciliopathy with hydrocephalus and randomization of left/right body asymmetry. *Am J Hum Genet*. 2019;105(5):1030-1039. http://doi.org/10.1016/j.ajhg.2019.09.022
25. Jin SC, Homsy J, Zaidi S, et al. Contribution of rare inherited and de novo variants in 2,871 congenital heart disease probands. *Nat Genet*. 2017;49(11):1593-1601. http://doi.org/10.1038/ng.3970
26. Kennedy MP, Omran H, Leigh MW, et al. Congenital heart disease and other heterotaxic defects in a large cohort of patients with primary ciliary dyskinesia. *Circulation*. 2007;115(22):2814-2821. http://doi.org/10.1161/CIRCULATIONAHA.106.649038
27. Shapiro AJ, Davis SD, Ferkol T, et al. Laterality defects other than situs inversus totalis in primary ciliary dyskinesia: insights into situs ambiguus and heterotaxy. *Chest*. 2014;146(5):1176-1186. http://doi.org/10.1378/chest.13-1704
28. Essner JJ, Amack JD, Nyholm MK, Harris EB, Yost HJ. Kupffer's vesicle is a ciliated organ of asymmetry in the zebrafish embryo that initiates left-right development of the brain, heart and gut. *Development*. 2005;132(6):1247-1260. http://doi.org/10.1242/dev.01663
29. Kramer-Zucker AG, Olale F, Haycraft CJ, Yoder BK, Schier AF, Drummond IA. Cilia-driven fluid flow in the zebrafish pronephros, brain and Kupffer's vesicle is required for normal organogenesis. *Development*. 2005;132(8):1907-1921. http://doi.org/10.1242/dev.01772
30. Shoemark A, Dixon M, Corrin B, Dewar A. Twenty-year review of quantitative transmission electron microscopy for the diagnosis of primary ciliary dyskinesia. *J Clin Pathol*. 2012;65(3):267-271. http://doi.org/10.1136/jclinpath-2011-200415
31. Fliegauf M, Olbrich H, Horvath J, et al. Mislocalization of DNAH5 and DNAH9 in respiratory cells from patients with primary ciliary dyskinesia. *Am J Respir Crit Care Med*. 2005;171(12):1343-1349. http://doi.org/10.1164/rccm.200411-1583OC
32. Olbrich H, Häffner K, Kispert A, et al. Mutations in DNAH5 cause primary ciliary dyskinesia and randomization of left-right asymmetry. *Nat Genet*. 2002;30(2):143-144. http://doi.org/10.1038/ng817
33. Djakow J, Svobodová T, Hrach K, Uhlík J, Cinek O, Pohunek P. Effectiveness of sequencing selected exons of DNAH5 and DNAI1 in diagnosis of primary ciliary dyskinesia. *Pediatr Pulmonol*. 2012;47(9):864-875. http://doi.org/10.1002/ppul.22520
34. Pennarun G, Escudier E, Chapelin C, et al. Loss-of-function mutations in a human gene related to Chlamydomonas reinhardtii dynein IC78 result in primary ciliary dyskinesia. *Am J Hum Genet*. 1999;65(6):1508-1519. http://doi.org/10.1086/302683
35. Onoufriadis A, Paff T, Antony D, et al. Splice-site mutations in the axonemal outer dynein arm docking complex gene CCDC114 cause primary ciliary dyskinesia. *Am J Hum Genet*. 2013;92(1):88-98. http://doi.org/10.1016/j.ajhg.2012.11.002
36. Narasimhan V, Hjeij R, Vij S, et al. Mutations in CCDC11, which encodes a coiled-coil containing ciliary protein, causes situs inversus due to dysmotility of monocilia in the left-right organizer. *Hum Mutat*. 2015;36(3):307-318. http://doi.org/10.1002/humu.22738
37. Ta-Shma A, Hjeij R, Perles Z, et al. Homozygous loss-of-function mutations in MNS1 cause laterality defects and likely male infertility. *PLoS Genet*. 2018;14(8):e1007602. http://doi.org/10.1371/journal.pgen.1007602
38. Lucas JS, Burgess A, Mitchison HM, et al. Diagnosis and management of primary ciliary dyskinesia. *Arch Dis Child*. 2014;99(9):850-856. http://doi.org/10.1136/archdischild-2013-304831

39. Horani A, Ferkol TW. Understanding primary ciliary dyskinesia and other ciliopathies. *J Pediatr*. 2021;230:15-22.e11. http://doi.org/10.1016/j.jpeds.2020.11.040
40. Wallmeier J, Nielsen KG, Kuehni CE, et al. Motile ciliopathies. *Nat Rev Dis Primers*. 2020;6(1):77. http://doi.org/10.1038/s41572-020-0209-6
41. Little RB, Norris DP. Right, left and cilia: how asymmetry is established. *Semin Cell Dev Biol*. 2021;110:11-18. http://doi.org/10.1016/j.semcdb.2020.06.003
42. Hou Y, Witman GB. The N-terminus of IFT46 mediates intraflagellar transport of outer arm dynein and its cargo-adaptor ODA16. *Mol Biol Cell*. 2017;28(18):2420-2433. http://doi.org/10.1091/mbc.E17-03-0172
43. Dai J, Barbieri F, Mitchell DR, Lechtreck KF. In vivo analysis of outer arm dynein transport reveals cargo-specific intraflagellar transport properties. *Mol Biol Cell*. 2018;29(21):2553-2565. http://doi.org/10.1091/mbc.E18-05-0291